Since January 2020 Elsevier has created a COVID-19 resource centre with free information in English and Mandarin on the novel coronavirus COVID-19. The COVID-19 resource centre is hosted on Elsevier Connect, the company's public news and information website.

Materials Science & Engineering C 117 (2020) 111323

Contents lists available at ScienceDirect

Materials Science & Engineering C

journal homepage: www.elsevier.com/locate/msec

Effects of cerium and tungsten substitution on antiviral and antibacterial properties of lanthanum molybdate

Takumi Matsumoto[a], Kayano Sunada[b], Takeshi Nagai[b], Toshihiro Isobe[a,*], Sachiko Matsushita[a], Hitoshi Ishiguro[b], Akira Nakajima[a,*]

[a] Department of Materials Science and Engineering, School of Materials and Chemical Technology, Tokyo Institute of Technology, 2-12-1 O-okayama, Meguro, Tokyo 152-8550, Japan

[b] Antibacterial and Antiviral Research Group, Kanagawa Institute of Industrial Science and Technology, LiSE4c-1, 3-25-13 Tonomachi, Kawasaki-ku, Kawasaki, Kanagawa 210-0821, Japan

ARTICLE INFO

Keywords:
Antibacterial
Antiviral
Ce
$La_2Mo_2O_9$
W

ABSTRACT

Powders of cerium (Ce)-substituted and tungsten (W)-substituted $La_2Mo_2O_9$ (LMO) were prepared using polymerizable complex method. Their antiviral and antibacterial performances were then evaluated using bacteriophage Qβ, bacteriophage Φ6, *Escherichia coli*, and *Staphylococcus aureus*. The obtained powders, which were almost single-phase, exhibited both antiviral and antibacterial properties. Effects of dissolved ions on their antiviral activity against bacteriophage Qβ were remarkable. A certain contribution of direct contact to the powder surface was also inferred along with the dissolved ion effect for antiviral activity against bacteriophage Φ6. Dissolved ion effects and pH values suggest that both Mo and W are in the form of polyacids. Antiviral activity against bacteriophage Φ6 was improved by substituting Ce for La in LMO. Similarly to LMO, Ce-substituted LMO exhibited hydrophobicity. Inactivation of alkaline phosphatase enzyme proteins was inferred as one mechanism of the antiviral and antibacterial activities of the obtained powders.

1. Introduction

The history of inorganic antiviral materials is not as long as that of organic antiviral materials. However, studies of inorganic antiviral materials are increasing gradually because one such material can affect various viruses under a wide temperature range with only a small probability of resistance development by a virus. Various materials have been investigated. Antiviral properties have been reported for metals [1–3] (e.g. Ag and Cu), photocatalysts (e.g. TiO_2 [4,5]), and other materials (e.g. ZnO and CaO [6,7]). In fact, some of these materials have already been applied for practical use. Nevertheless, these materials entail several difficulties such as coloration or inactivation because of oxidation, and usage environment restrictions (requirement of light illumination, or alkalization). Development of new inorganic antiviral materials has been demanded to overcome these and other difficulties.

We specifically examined the hydrophobicity of rare-earth oxides [8–12] and antibacterial effects of molybdenum [13–16]. Then we developed the complex oxide $La_2Mo_2O_9$ (hereinafter LMO) using polymerizable complex method [17]. This material exhibited hydrophobicity and simultaneous antibacterial effects against gram-negative (*Escherichia coli*, *E. coli*) and gram-positive (*Staphylococcus aureus*, *S. aureus*) bacteria, and antiviral effects against non-envelope (bacteriophage Qβ, hereinafter denoted as Qβ) and envelope (bacteriophage Φ6, hereinafter denoted as Φ6) viruses [18]. Moreover, both antibacterial and antiviral activities were found to be greater than two orders after 6 h in the dark. However, the material's antiviral activity against Φ6, which is similar to influenza and COVID-19 viruses, was less than that against *E. coli*, *S. aureus*, or Qβ.

Given this background, we tried to substitute different atoms into LMO to improve its antiviral activity against Φ6 type viruses. We selected cerium (Ce) and tungsten (W) because CeO_2 exhibits antibacterial activity and because it is a readily available, low-cost rare-earth oxide [19–22]. Tungsten, located below Mo in the periodic table, forms a solid solution with Mo in a wide chemical composition range [23,24]. Our preliminary experiments conducted using these two elements revealed that single-phase powder was difficult to obtain for high Ce concentrations. As the W concentration increases, the antibacterial performance of the material is degraded. Therefore, for this study, we replaced 10% of La with Ce ($La_{1.8}Ce_{0.2}Mo_2O_9$, hereinafter denoted as LCMO) and 50% of Mo with W ($La_2(Mo, W)O_9$, hereinafter denoted as LMWO). These powders were prepared using the same polymerizable

* Corresponding authors.
E-mail addresses: isobe.t.ad@m.titech.ac.jp (T. Isobe), nakajima.a.aa@m.titech.ac.jp (A. Nakajima).

https://doi.org/10.1016/j.msec.2020.111323
Received 29 April 2020; Received in revised form 20 July 2020; Accepted 30 July 2020
Available online 04 August 2020

complex method as that used for an earlier study [18]. Then we compared their performance with that of LMO.

2. Experiment procedure

2.1. Powder synthesis and characterization

As starting materials for this study, we used lanthanum (III) nitrate hexahydrate ($La(NO_3)_3{\cdot}6H_2O$, 99.9%), hexa-ammonium heptamolybdate tetrahydrate ($(NH_4)_6Mo_7O_{24}{\cdot}4H_2O$, 99.9%), ammonium tungstate pentahydrate ($(NH_4)_{10}W_{12}O_{41}{\cdot}5H_2O$, 85%), and cerium (III) nitrate hexahydrate ($Ce(NO_3)_3{\cdot}6H_2O$, 99.9%), all from Fujifilm Wako Pure Chemical Corp., and all with no further purification.

For LMO, $La(NO_3)_3{\cdot}6H_2O$ (2.50 g) and $(NH_4)_6Mo_7O_{24}{\cdot}4H_2O$ (1.02 g) were each dissolved into distilled water (10 ml). Then these solutions were mixed such that La:Mo = 1:1. For LMWO, $(NH_4)_6Mo_7O_{24}{\cdot}4H_2O$ (0.51 g) and $(NH_4)_{10}W_{12}O_{41}{\cdot}5H_2O$ (0.754 g) were each dissolved into distilled water (20 ml). After $La(NO_3)_3{\cdot}6H_2O$ (2.50 g) was dissolved into distilled water (10 ml), these solutions were mixed to set La:(Mo + W) = 1:(0.5 + 0.5). For LCMO, $La(NO_3)_3{\cdot}6H_2O$ (2.25 g) and $Ce(NO_3)_3{\cdot}6H_2O$ (0.250 g) were each dissolved into distilled water (8 ml for $La(NO_3)_3{\cdot}6H_2O$ and 2 ml for $Ce(NO_3)_3{\cdot}6H_2O$). In addition, $(NH_4)_6Mo_7O_{24}{\cdot}4H_2O$ (1.02 g) was dissolved into distilled water (10 ml). These solutions were then mixed to set (La + Ce):Mo = (0.9 + 0.1):1.

Subsequently, 2.31 mol/l of citric acid ($C_6H_8O_7$, 99.5%; Fujifilm Wako Pure Chemical Corp.) aqueous solution was added to the mixed solution. The molar ratio of metal ion (La + Ce + Mo + W) to citric acid was 1:2. Then it was stirred for 10 min. Ethylene glycol ($C_2H_6O_2$, 99.5%; Fujifilm Wako Pure Chemical Corp.) was added to the solution so that the molar ratio of ethylene glycol to citric acid was 2:3. This solution was stirred in a water bath at 80 °C for 6 h to facilitate esterification. Then precursor gels were obtained. The obtained gels were dried at 200 °C in ambient air. The dried gels were milled for 10 min using a mortar and pestle. After calcination at 500 °C (LMO) or 550 °C (LMWO, LCMO) for 12 h in ambient air, LMO, LMWO and LCMO powders were obtained.

The microstructures of the obtained powders were observed using a field-emission scanning electron microscope (FE-SEM, JSM7500F; JEOL, Japan) and a transmission electron microscope (TEM, JEM-2010F; JEOL, Japan). The specific surface area of each powder was measured using Brunauer–Emmett–Teller (BET) method with N_2 (BEL SORP mini; MicrotracBEL Corp., Japan). The crystalline phase of the powders was evaluated using X-ray diffraction (XRD, XRD-6100; Shimadzu Corp., Japan) with a Cu Kα radiation source. The UV–vis absorption spectra of the samples were obtained using a UV–vis scanning spectrophotometer (V-660; Jasco Corp., Tokyo, Japan). Barium sulfate powder was used as a reference for this measurement. The chemical composition of the powders was evaluated using inductively coupled plasma analysis (ICP-OES, 5100 VDV; Agilent Technologies Japan Ltd., Tokyo, Japan) and an X-ray photoelectron spectroscope (XPS, Quantera SXM; Ulvac-Phi Inc., Japan) with an Al Kα X-ray line (1486.6 eV).

2.2. Antiviral and antibacterial activity measurements

2.2.1. Sample preparation

For this study, antiviral and antibacterial activity measurements were taken not only for prepared powders but also for La_2O_3 (99.99%; Fujifilm Wako Pure Chemical Corp.), CeO_2 (99.5%; Fujifilm Wako Pure Chemical Corp.), WO_3 (> 99%; Kanto Chemical Co. Inc., Tokyo, Japan), and MoO_3 (99.0%; Fujifilm Wako Pure Chemical Corp.). All these oxide reagents were washed in distilled water (powder:water = 5 g:500 ml) and were dried at 100 °C for 12 h before measurements. These powder samples were dispersed into ethanol (sample:ethanol = 1 mg:1 ml; C_2H_6O, 99.5%; Fujifilm Wako Pure Chemical Corp.). The suspension (0.15 ml) was loaded uniformly onto a glass substrate (25 mm × 25 mm) and was dried at 100 °C for 30 min. After the loading–drying cycle was repeated three times, the substrate was coated with the sample powder (0.45 mg total amount).

2.2.2. Antiviral activity measurement

2.2.2.1. Film adhesion method. We used Qβ (NBRC 20012) and Φ6 (NBRC 105899) as viruses for antiviral activity measurements. Stock suspensions of Qβ and Φ6 were prepared according to ISO 18061. The stock phage suspension was resuspended to ca. 2.0×10^7 plaque-forming units (PFU)/mL in 1/500 nutrient broth (1/500 NB; Eiken Chemical Co. Ltd., Tokyo, Japan) that was 1 × NB 500-fold dilution with sterile water. A 50 μl ($=10^6$ PFU) phage suspension was pipetted onto a substrate with the sample powder and was covered with a transparent film (20 mm × 20 mm, VF-10; Kokuyo Co. Ltd., Osaka, Japan) to contact the suspension with the sample powder. Then it was incubated under humid conditions at room temperature (ca. 25 °C) in a dark room for 0, 2, 4, or 6 h. After incubation, the phages were harvested by shaking with 10 ml soybean casein digest broth with lecithin and polysorbate broth (SCDLP; Eiken Chemical Co. Ltd., Tokyo, Japan) for 2 min to stop the incubation.

The Qβ or Φ6 in SCDLP was diluted with 0.01 M phosphate buffered saline (PBS; Sigma-Aldrich Corp., USA) solution. We used *E. coli* (NBRC 106373) and *Pseudomonas syringae* (NBRC 14084, *P. syringae*), respectively, as host bacteria for Qβ and Φ6. Both Qβ and Φ6 were infected respectively with *E. coli* and *P. syringae* for 10 min. Subsequently, the infected bacteria suspension (1 ml) was mixed with 0.5% Luria broth agar (LB; Nacalai Tesque Inc., Kyoto, Japan and agar; Fujifilm Wako Pure Chemical Corp.). Then the mixture was spread out on 1.5% LB agar plate to form a double agar layer. The plate was incubated at 37 °C for 48 h to form the plaques. The titer after incubation (N) was calculated by counting the plaques. Control data were obtained using the same experimental procedure with a pristine glass plate instead of glass plates with sample powders. The plaque assay was performed twice for each point. Hereinafter, we designate this method as the film adhesion method.

2.2.2.2. Dissolved ion contact method. As described also for an earlier study, we evaluated the ion concentration when dissolved into 1/500 NB. To elucidate the contribution of dissolved ions to the overall antiviral activity, we took antiviral activity measurements using the solution after filtering the powder samples. Each prepared powder was mixed with 1/500 NB by the same solid–liquid ratio as that used for the film adhesion method. Then the mixture was shaken at 100 times/min for 2 h. Each suspension was filtered to exclude the powder. The pH value of the filtrate was measured. In addition, the amount of the dissolved ion (La, Ce, W, and Mo) was measured using ICP-OES. The filtrate solution was used for antiviral activity measurements against Qβ and Φ6. The filtrate solution, the suspensions of Qβ or Φ6 (2.2×10^7 PFU/ml), and the distilled water were mixed at a ratio of 8:1:1. This mixture was stirred and incubated at room temperature (ca. 25 °C) in the dark for 2, 4, and 6 h. After incubation, the reaction was stopped with SCDLP medium. The medium was diluted with 0.01 M PBS. Then the antiviral activity was evaluated using the same procedure as that used for the film adhesion method. The initial virus concentration before contact with the filtrate solution including dissolved ions was set as the 0 h value. The control data were obtained using 1/500NB instead of the filtrate solution. Therefore, the ratio of 1/500NB, the virus suspensions, and the distilled water was 8:1:1; then, the same measurements were conducted. Hereinafter, this method is described as the dissolved ion contact method.

2.2.3. Antibacterial activity measurement

Evaluation of the antibacterial activity was conducted according to a film adhesion method described for ISO 17094, with minor modifications. For this study, we used *E. coli* (NBRC 3972) and *S. aureus* (NBRC 12732). Each had been precultured on nutrient agar (NA; Nissui

Pharmaceutical Co. Ltd., Tokyo, Japan) at 37 °C for 18 h and had been suspended in 1/500 NB. The concentrations of these bacteria were fixed to ca. 2.0 × 10^6 colony-forming units (CFU)/ml. A 50 μl (=10^5 CFU) bacteria suspension was pipetted onto a substrate loaded with the sample powder. After the substrate was covered with a transparent film to contact the bacteria suspension with the particles, it was incubated under a humid condition at room temperature (ca. 25 °C) in a dark room. After a certain period (0, 2, 4, and 6 h), the bacteria were harvested by shaking with 5 ml SCDLP for 2 min to halt the incubation. The bacteria in SCDLP were diluted with 0.01 M PBS. Each 1 ml of the diluted bacteria suspension was mixed in NA and was incubated at 37 °C for 48 h to produce bacterial colonies. The concentration of viable bacterial cells at each time point (*N*) was calculated by multiplying the number of colonies and the dilution ratio. The control cell concentrations were calculated using the same procedure as that used for a pristine glass substrate. The initial cell concentration for each sample was presented as the cell concentration at 0 h. The colony assay was conducted twice for each point.

2.2.4. Cytotoxicity test

Cytotoxicity confirmation was conducted using Madin–Darby canine kidney cells (MDCK cells, CCL-34) purchased from American Type Culture Collection (Manassas, VA, U.S.A.). Cells were maintained using modified Eagle's medium containing 10% fetal bovine serum and were incubated at 35 °C under a humidified 5% CO_2 atmosphere in an incubator. The prepared sample glass was put in a Petri dish into which was poured 5 ml of PBS. The extraction solutions of sample powders were prepared by shaking 100 times/min for 2 h. The extraction solution (50 μl) and MDCK cell solution (4.0 × 10^5 cells/ml, 150 μl) were mixed and incubated at 35 °C under a humidified 5% CO_2 atmosphere in an incubator for 4 days. After incubation, an adenosine triphosphate detection reagent (Viral ToxGlo™ Assay; Promega Corp., U.S.A.) was added (100 μl). A spectrophotometer (infiniteM200; Tecan Group Ltd., Austria) was used to measure the emitted light intensity. The number of living cells was calculated. Control data were obtained using the same experimental procedure with a pristine glass plate used instead of a glass plate with a sample powder.

3. Results and discussion

3.1. Powder characterization

Fig. 1 presents XRD patterns of the prepared powders. The obtained powders were almost single phase; peaks in the patterns were identified as $La_2Mo_2O_9$ (card No. 28-0509). Fig. 2 portrays the corresponding SEM micrographs. The primary particle sizes of the powders were 50–100 nm. No specific microstructure such as micro domains was observed in these particles by TEM observation (see Fig. SI-1 in Supporting information). XRD patterns and SEM micrographs of oxide reagents are presented in Supporting information (Figs. SI-2 and 3). They were larger than the prepared powders. Although La_2O_3 was the

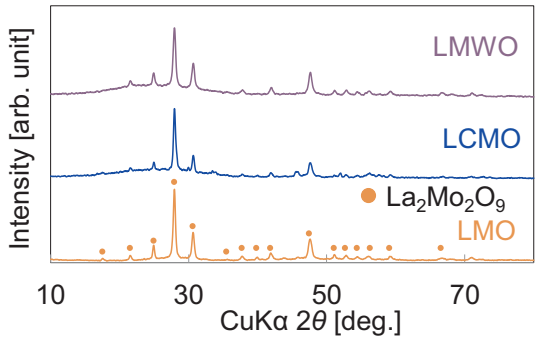

Fig. 1. XRD patterns of prepared powders.

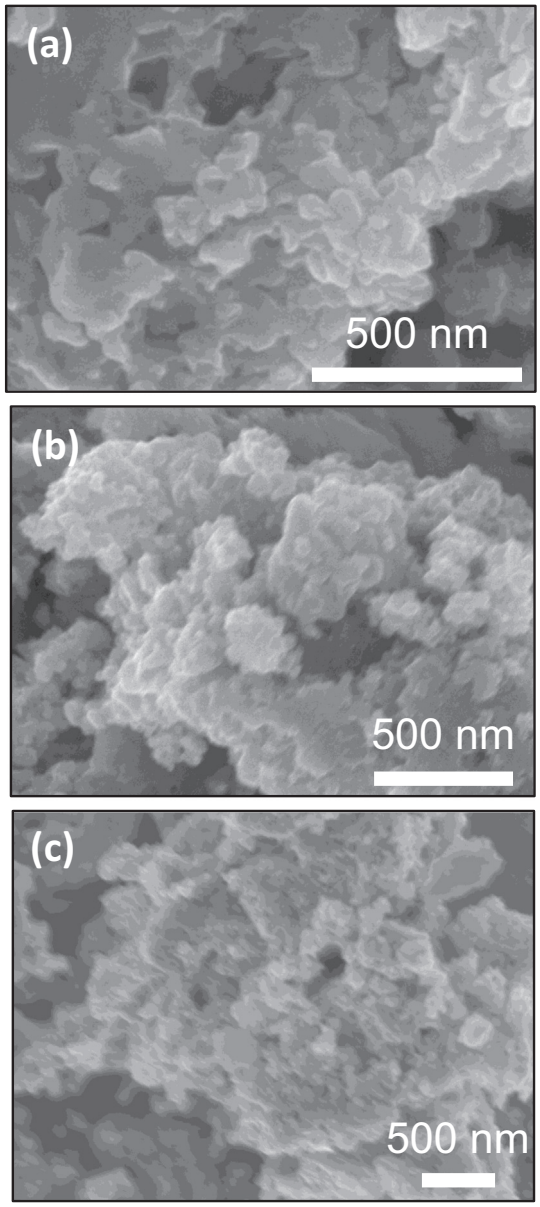

Fig. 2. SEM micrographs of prepared powders: (a) LMO, (b) LCMO, and (c) LMWO.

mixture of La_2O_3 (card No. 5-0602, major phase) and $La(OH)_3$ (card No. 5-0585, minor phase), others were single-phase oxides. Their peaks were identified respectively as CeO_2 (card No. 34-0394), MoO_3 (card No. 5-0508), and WO_3 (card No. 32-1395).

Subsequent ICP analysis revealed that all prepared powder samples possess the chemical composition ratio as charged (La:Mo = 1:1 for LMO, La:Ce:Mo = 1.7:0.2:2.0 for LCMO, and La:Mo:W = 1.9:1.0:1.0 for LMWO, respectively). In the wide scan XPS spectra, only constituent elements and carbon were detected. Narrow scans were conducted on La3d, Ce3d, Mo3d, and W4f, respectively (see Fig. SI-4 in Supporting information). Surface compositions for the prepared powder samples obtained by XPS were La:Mo = 0.9:1 for LMO, La:Ce:Mo = 1.7:0.2:2.0 for LCMO, and La:Mo:W = 1.8:1.0:1.0 for LMWO. The amount of Mo + W was slightly richer than that of La + Ce at the powder surface. This result might be because of the solubility difference among these elements and suggests the formation of cation vacancy in the surface. However, the composition difference XPS and ICP was not significant. The valences of La, Mo, and W were identified as La(III), Mo(VI), and W (VI) [25–27]. For Ce, although S/N ratio of the spectrum was small, it

Table 1
Results of pH and dissolved ion concentration in 1/500 NB solution, with specific surface areas of prepared powders and oxide reagents.

	pH	SSA [m^2/g]	La [μmol/l]	Ce [μmol/l]	Mo [μmol/l]	W [μmol/l]
Initial	7.80	–	–	–	–	–
LMO	5.26	6.8	168	N.D.	299	N.D.
LCMO	5.77	10.4	75	0.43	112	N.D.
LMWO	5.84	12.0	12	N.D.	16	1
La_2O_3	6.60	0.6	2	N.D.	N.D.	N.D.
MoO_3	3.35	1.7	N.D.	N.D.	3992	N.D.
CeO_2	5.46	3.3	N.D.	4	N.D.	N.D.
WO_3	4.87	4.8	N.D.	N.D.	N.D.	87

was identified as Ce(III):Ce(IV) = 56:44 by the deconvolution of Ce3d peaks [28,29].

Table 1 presents results of pH and dissolved ion concentrations from sample powders immersed in 1/500 NB, and presents the specific surface areas of samples. The surface area values were 7–12 m^2/g for prepared powders. The bar graphs for pH and dissolved ion concentrations presented in Table 1 are displayed in Supporting information (Figs. SI-5 and SI-6). The initial pH value for 1/500 NB before ion dissolution from the powders was 7.8. Despite their small specific surface areas, the dissolved ion concentrations from MoO_3, CeO_2, and WO_3 were greater than those from prepared powders. The solubility of MoO_3 in water is 3.4 mmol/l at 28 °C [30]. Results obtained for La_2O_3, CeO_2, and WO_3 are quite low. They can indicate that the materials are almost insoluble [31,32]. The dissolved ion concentration found for La_2O_3 was the lowest among oxide reagents. Dissolved amounts of Ce, W, and Mo decreased because they formed complex oxides with La. This result implies that the dissolution of Ce, W, and Mo was suppressed, and that the sustained release of these elements is attributable to the formation of complex oxides with La because of its low solubility. The dissolved ion amount ratios between La and Mo are of almost equal order, which suggests that the dissolution of Mo induces La dissolution. An inverse trend was found between pH values and the Mo dissolution amount. As described in an earlier report [18], that result is expected to be attributable to the resultant increase of the hydronium ion concentration by Mo dissolution. The pH value order for oxide reagents was $La_2O_3 > CeO_2 > WO_3 > MoO_3$. By forming complex oxides with La, the pH values of prepared powders became higher than those of simple oxide reagents.

3.2. Antiviral activity

Fig. 3 presents results of antiviral activity against Qβ for prepared powders (Fig. 3(a) and (b)) and oxide reagents (Fig. 3(c) and (d)) obtained by film adhesion method (Fig. 3(a) and (c)) and dissolved ion contact method (Fig. 3(b) and (d)). The antiviral activity achieved using dissolved ion contact method was higher than that achieved using film adhesion method for LMO, LCMO, and LMWO. The trend found for LMO and LMWO was similar to that found for oxide reagents. Although little antiviral activity was found for CeO_2, La_2O_3 exhibited clear antiviral activity against Qβ. The antiviral activity order by film adhesion method was $MoO_3 > WO_3$, and $La_2O_3 > CeO_2$; that by dissolved ion contact method was La_2O_3, $WO_3 > MoO_3 > CeO_2$.

The contributions of dissolved ions, especially those of ions of La, W, and Mo, are large for antivirus activity against Qβ because the activity achieved using dissolved ion contact method was higher than that achieved using film adhesion method. Before this study, we conducted a preliminary study of $LaVO_4$, for which we replaced Mo by V in LMO. This material exhibited a small pH value (4.71) under the same experiment conditions. Because the dissolved amount of V is much greater than that of La, ion exchange between VO_4^{3-} and OH^- were expected for charge compensation. Nevertheless, this material exhibited little antiviral or antibacterial activity (see Table SI-1, Figs. SI-7 and SI-8 in Supporting information). Consequently, differences of antiviral activity cannot be attributed simply to the different pH values.

The dissolved W and Mo form polyacids in this pH range. They might form heteropolyacids with other ions because the solution contains various ions such as phosphorous. The polyacids have a negative charge in aqueous media and contribute to antiviral activity [33–36]. Judd et al. demonstrated that polyacids adsorbed at the cation site of lysine residue in the active site of reverse transcriptase by electrostatic interaction and demonstrated that they inactivate human immunodeficiency virus (HIV) [37]. Reportedly, lysine residue is necessary for bonding with proteolytic enzymes in neuraminidase, which contributes to desorption from the host cell [38]. These polyacids might contribute to inactivation by inhibiting virus desorption from the host cell. Although HIV is a virus with an envelope, lysine residue also exists on the surface of non-envelope viruses at the active site of a spike, which contributes to bonding with the host cell [39]. Actually, lysine residue exists in the structure of Qβ [40]. Consequently, these polyacids can be expected to contribute also to inactivation of non-envelope viruses such as Qβ.

Several reports have described adsorption or interaction between Mo or W ion (strictly speaking, poly type anions of molybdate (MoO_4^{2-}) or tungstate (WO_4^{2-}) ions) and lysine under different pH [41–43]. The adsorption amount of Mo and W polyacids to lysine depends on the lysine–metal ratio. The adsorption amount of W exceeds that of Mo when the ratio becomes higher than a certain value [43]. This ratio might engender antiviral activity difference between WO_3 and MoO_3 in dissolved ion contact method. Pérez et al. demonstrated that La(III) does not enter the host cell. It blocks Ca(II) entry induced by rotavirus (non-envelope type virus) infection [44]. Wengler et al. also demonstrated that lanthanide ion (such as La(III) and Ce(III)) treatment blocks the ability of the host cell to support the replication of flavivirus (envelope type virus) RNA. A similar effect of La(III) is expected to contribute to the inactivation of Qβ [45]. The slight antiviral activity shown by CeO_2 might be attributable to the major Ce ion valence (not III but IV).

Based on the relation between the dissolved ion amount and antiviral activity against Qβ, we can infer that the activity order of prepared powders depends on the dissolved ion amount, and especially on the amounts of La and Mo. The dissolved La(III) amount was LMO > LCMO > LMWO > La_2O_3, whereas antiviral activity by dissolved ion contact method was La_2O_3, $WO_3 \approx$ LMO > LCMO > LMWO $\gg CeO_2$. The activity difference between WO_3 and LMWO is attributable to the dissolved W ion concentration difference. However, the activity order of LMO, LCMO, LMWO, and La_2O_3 does not simply follow the order of the dissolved La amount. Although the reason for this result remains unclear, one reasonable explanation is the interaction among La, W, and Mo ions. The antiviral effects of La ion against Qβ might weaken when W or Mo ions co-exist in the solution by formation of heteropolyanion; alternatively, they might weaken for some other reason.

Fig. 4 presents the results of antiviral activity against Φ6 for prepared powders (Fig. 4(a) and (b)) and oxide reagents (Fig. 4(c) and (d)) by film adhesion method (Fig. 4(a) and (c)) and by dissolved ion contact method (Fig. 4(b) and (d)). The antiviral activity achieved by dissolved ion contact method was lower than that achieved by film adhesion method for LMO, LCMO, and LMWO. The antiviral activity order shown by film adhesion method was LCMO > LMWO > LMO. That by dissolved ion contact method was LCMO > LMO > LMWO. The activity order of oxide reagents was $MoO_3 > WO_3 \gg La_2O_3 > CeO_2$. This order was the same for both methods. Although the antiviral activity of WO_3 by dissolved ion contact method is higher than that by film adhesion method, other oxide reagents exhibited similar antiviral activity from these two methods.

Dissolved Mo and W ion also contribute to the overall antiviral activity against Φ6 to some degree, although their contributions are not

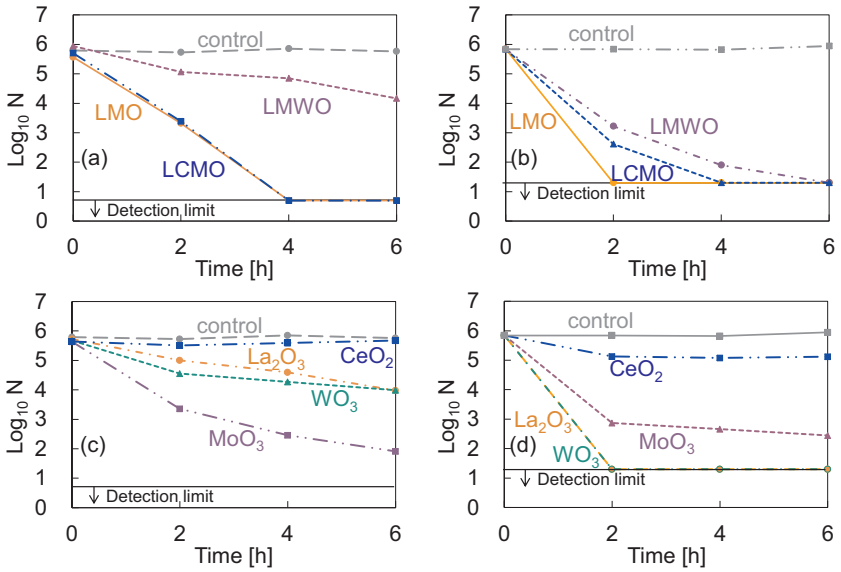

Fig. 3. Results of antiviral activity against Qβ for prepared powders ((a) and (b)) and oxide reagents ((c) and (d)): (a) and (c), film adhesion method; and (b) and (d), dissolved ion contact method.

as strong as that of Qβ. The antiviral activity by dissolved ion contact method was lower than that by film adhesion method for prepared powders. Therefore, we can infer that the effects of direct contact of the virus to the powder surface also exist for these powders. This trend differs from Qβ. The ion concentration is expected to be high around the powder surface. Therefore, this difference might be attributable to the difference of virus characteristics such as the resistance against dissolved ions. Resistance against La ion might also be related to this difference. The addition of Ce ion shows positive effects on antiviral activity against Φ6. In fact, LCMO exhibited the highest activity among the prepared powders, even though the dissolved ion amount is less than that for LMO. Because CeO_2 possesses little antiviral activity, some synergetic effect is expected between Ce and Mo ions.

To date, several investigations have been conducted to elucidate the antiviral activity of polyacids combined with rare-earth elements [46–48]. Liu et al. investigated antiviral activity against influenza viruses (envelope type viruses similar to Φ6) of rare-earth borotungstate heteropolyoxometalates. They demonstrated that heteropoly blues (a part of W in polyacid that is reduced) containing Ce exhibits the strongest inhibition activity against influenza virus. They inferred that this substance has a molecular size that is suitable to interfere and destroy the virus or virus' chemical components [47]. Recently, Shiohara et al. and Kato et al. demonstrated that a combination of multi-valence elements such as Mn and Ni enhances the Mars – van Krevelen mechanism [49,50], which derives from the strong oxidation power of Ce [51,52]. Actually, when LCMO was washed with ethanol, the ratio of Ce(IV) decreased and that of Mo(V) increased (see Fig. SI-9 in Supporting information). Therefore, the oxidation power of Ce might also enhance antiviral activity against Φ6. Further investigations must be conducted to identify the dominant mechanism of this system. However, the effect of Ce is more remarkable on Φ6 than on Qβ. The combination of Ce ion and Mo-based polyacids is expected to be advantageous for similar viruses such as influenza and COVID-19.

For this study, the advantage of W for antiviral activity by film

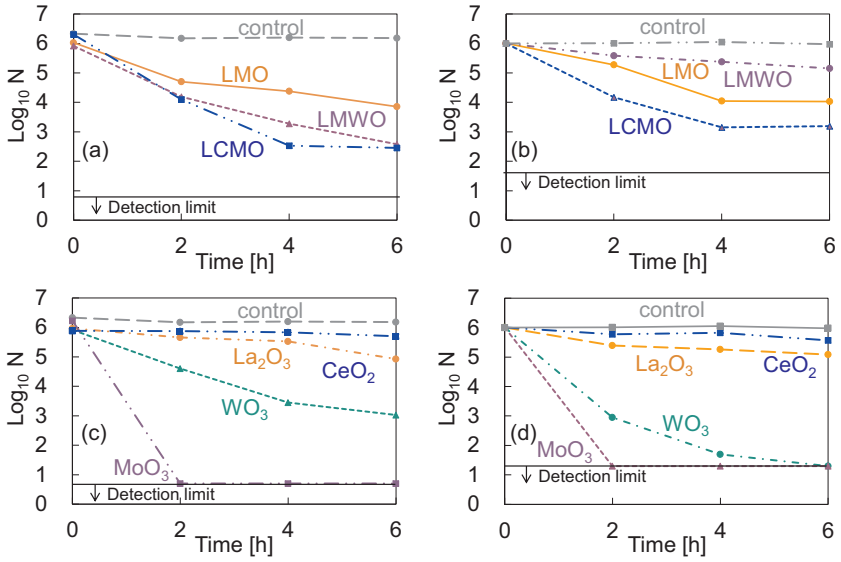

Fig. 4. Results of antiviral activity against Φ6 for prepared powders ((a) and (b)) and oxide reagents ((c) and (d)): (a) and (c), film adhesion method; and (b) and (d), dissolved ion contact method.

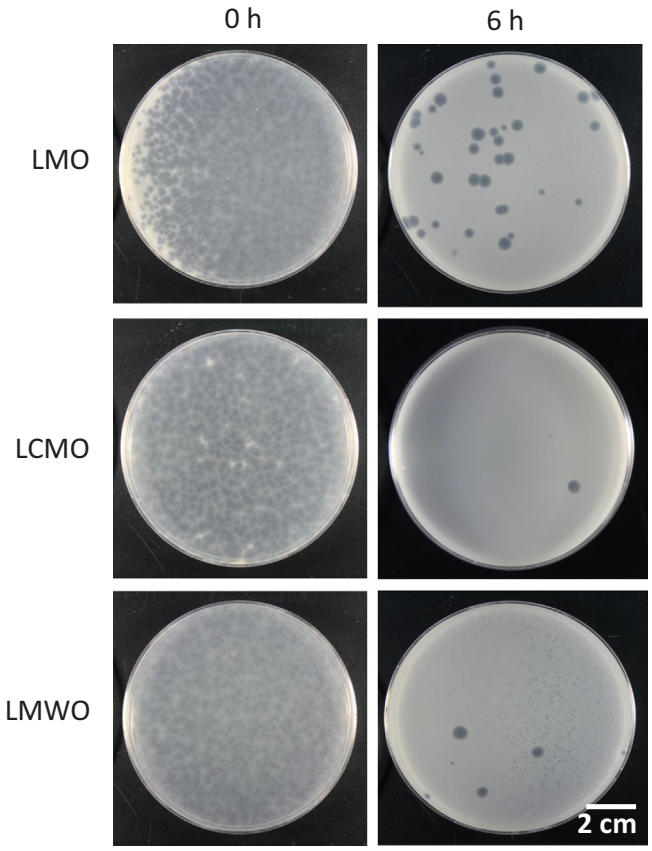

Fig. 5. Photographs of the change of plaque number for Φ6 by film adhesion method.

adhesion method (LMWO > LMO) is remarkable. However, a different trend was obtained when dissolved ion contact method (LMO > LMWO) was used. The dissolved ion amount for LMWO is much smaller than that of LMO, probably because of the decrease of the atomic ratio of Mo with high solubility. Near the powder surface, the ion concentration increases. For that reason, the effect of direct contact of the virus to the surface becomes remarkable; LMWO exhibited higher antiviral activity than LMO by film adhesion method. Therefore, if the direct contact situation between powder and virus is designed effectively, then W addition might also be effective for increasing antiviral activity against Φ6.

Fig. 5 displays photographs of the change of plaque number for Φ6 that occurs when using film adhesion method. The number of plaques was decreased remarkably. Almost all plaques were eliminated by LCMO within 6 h.

3.3. Antibacterial activity

Fig. 6(a) and (b) presents results of antibacterial activity against *E. coli* for prepared powders (Fig. 6(a)) and for oxide reagents (Fig. 6(b)). The activity order for the prepared powders was LMO > LCMO ≈ LMWO. That for oxide reagents was MoO_3 > La_2O_3 ≫ WO_3, CeO_2. Antibacterial activity was not obtained from WO_3 or CeO_2.

Several studies have examined the antibacterial activity of La_2O_3 [53–55]. The mechanism was attributed to nutritional inhibition by the absorption of phosphoric acids [54,55]. Actually, LMO exhibited higher activity than that of either La_2O_3 or MoO_3, which suggests synergic effects of La and Mo. We conducted alkaline phosphatase (ALP) enzyme inactivation testing to investigate the antibacterial activity mechanism. Detailed experiment procedures were described in *Supporting information*. The ALP is a kind of enzyme protein with a higher-order structure formed by three-dimensional combinations of long molecular chains of 20 amino acids. When a change of the molecular interaction from some external cause distorts the higher-order structure, protein functions degrade and deactivate [56]. The result is portrayed in Fig. 7. This figure presents the antibacterial activity rate ($\log_{10}(N/N_0)$/h) against *S. aureus*. Results show that MoO_3, La_2O_3, LMWO, LCMO, and LMO provided high ALP inactivation rates. This trend roughly corresponds to the antibacterial activity rate, which implies that inactivation of the enzyme proteins such as ALP is one mechanism of antibacterial activity for these powders. Sunada et al. investigated the antiviral performance of Cu_2O and demonstrated that Cu_2O possesses ALP enzyme inactivation activity [57,58]. They inferred the antiviral performance of their materials as derived from this activity because the outer part of the virus is made of protein. Some are proteins necessary for adsorption and release to host cells. Therefore, the ALP inactivation activity of these samples is expected to contribute to their antiviral activity.

Fig. 6(c) and (d) respectively presents results of antibacterial activity against *S. aureus* obtained for the prepared powders and oxide reagents. The activity order for the prepared powders was LMO > LCMO ≈ LMWO. That for oxide reagents was MoO_3 > La_2O_3 ≫ WO_3, CeO_2. Antibacterial activity was not exhibited by either WO_3 or CeO_2.These trends are almost identical to that found for *E. coli*, which suggests that substitution of Ce or W for the part of LMO is ineffective for antibacterial activity improvement. However, both LCMO and LMWO retain a certain degree of antibacterial activity (three order decrease in 6 h). Fig. 8 displays the cytotoxicity test results for LMO, LCMO, and LMWO. None of these powders possesses cytotoxicity. This result was the same as that obtained from our previous study [18]. It is noteworthy that various experiments can be used to assess the toxicity of the materials. Further various experiments are necessary to confirm the cytotoxicity of these materials.

The dissolved amount of ions from prepared powders is greater than that for oxidized silver (Ag_2O, 0.86 μmol/l [59]), but less than that for MoO_3. All these powders are white (LMO and LMWO) or light yellow (LCMO). The probability of spoiling design is low. Although MoO_3 is effective for antiviral and antibacterial use in the initial stage, its activity is expected to deteriorate quickly because of its high solubility. Actually, La-based complex oxides such as LMO, LCMO, and LMWO are difficult to deactivate. For that reason, they retain their activity longer than MoO_3, releasing Mo-polyacids slowly with higher amounts of minimal inhibitory concentration (MIC) value (0.17–1.7 μmol/l for *E. coli* [60]).

This study indicated LCMO as the most promising material with high antiviral activity against Φ6. We confirmed that this material possesses not only antiviral and antibacterial properties but also hydrophobicity similar to that of LMO (see Figs. SI-10, SI-11, and SI-12 in Supporting information). Because of its hydrophobicity, this complex oxide is expected to have good affinity with organic compounds. It is noteworthy that the method of measuring antiviral and antibacterial properties used for this study does not include the contribution of materials' hydrophobicity. Several earlier studies demonstrated the benefits of hydrophobicity for antiviral and antibacterial performance [61–63]. Detailed investigations of the relations between hydrophobicity and antiviral or antibacterial performance of this material must be undertaken in future work.

Unlike LMO, LCMO has a UV-shielding property that originated in Ce [64–66] (Fig. 9). However, photocatalytic decomposition activity was not obtained from this material. Therefore, this material might be applicable to UV shielding coatings for windows or cosmetics.

4. Summary

For this study, we partially replaced La and Mo of $La_2Mo_2O_9$ (LMO) by Ce or W. We then investigated their antiviral and antibacterial properties using Qβ, Φ6, *E. coli*, and *S. aureus*. The powdered sample was prepared using polymerizable complex method. The obtained

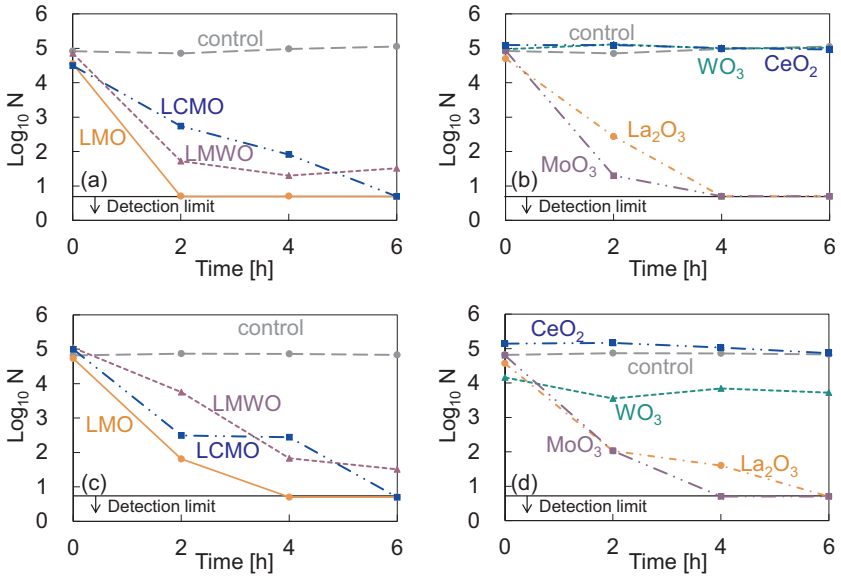

Fig. 6. Results of antibacterial activity for powders and oxide reagents prepared using film adhesion method: (a) *E. coli* by prepared powders, (b) *E. coli* by oxide reagents, (c) *S. aureus* by prepared powders, and (d) *S. aureus* by oxide reagents.

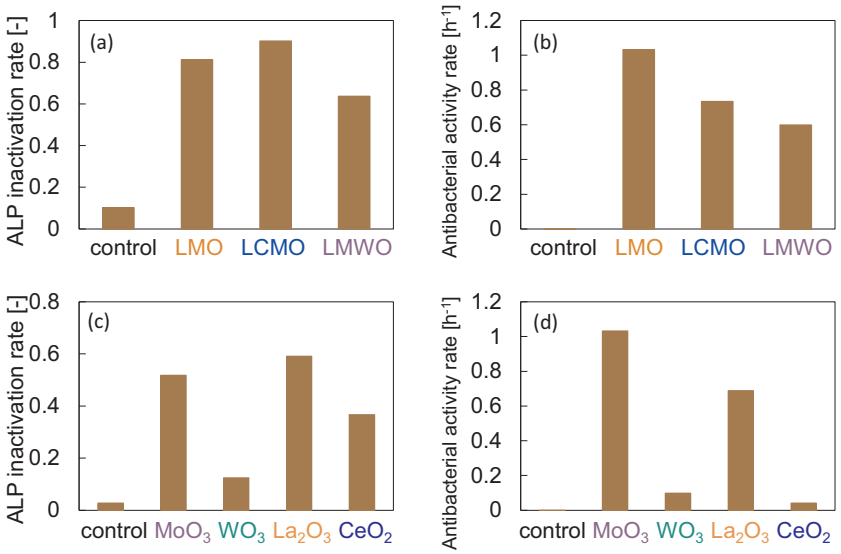

Fig. 7. ALP inactivation rate ((a) and (c)), and antibacterial activity rate against *S. aureus* ((b) and (d)) for prepared powders and oxide reagents.

powders, which were almost single phase, exhibited both antiviral and antibacterial performance. The dissolved ions strongly affect antiviral activity against Qβ. A certain contribution of direct contact between the powder surface and virus was inferred, aside from the effects of dissolved ions for antiviral activity against Φ6. Results suggest that Mo and W form polyacids in the solution. Partial substitution of Ce for La improved the antiviral activity against Φ6. All prepared powders inactivated ALP enzyme proteins, suggesting that one mechanism accounts for their antiviral and antibacterial performance.

CRediT authorship contribution statement

Takumi Matsumoto: Investigation, Data curation, Formal analysis
Kayano Sunada: Investigation, Methodology, Data curation
Takeshi Nagai: Methodology
Toshihiro Isobe: Investigation, Supervision
Sachiko Matsushita: Investigation
Hitoshi Ishiguro: Methodology, Data curation, Formal analysis
Akira Nakajima: Conceptualization, Project administration, Supervision.

Declaration of competing interest

The authors declare that they have no known competing financial interests or personal relationships that could have appeared to influence the work reported in this paper.

Acknowledgments

The authors are grateful to the staff of the Center of Advanced Materials Analysis (CAMA) at the Tokyo Institute of Technology for various characterizations and for helpful discussion related to this study. This work was supported in part by the KOSÉ Cosmetology Research Foundation and the IKETANI Science and Technology Foundation.

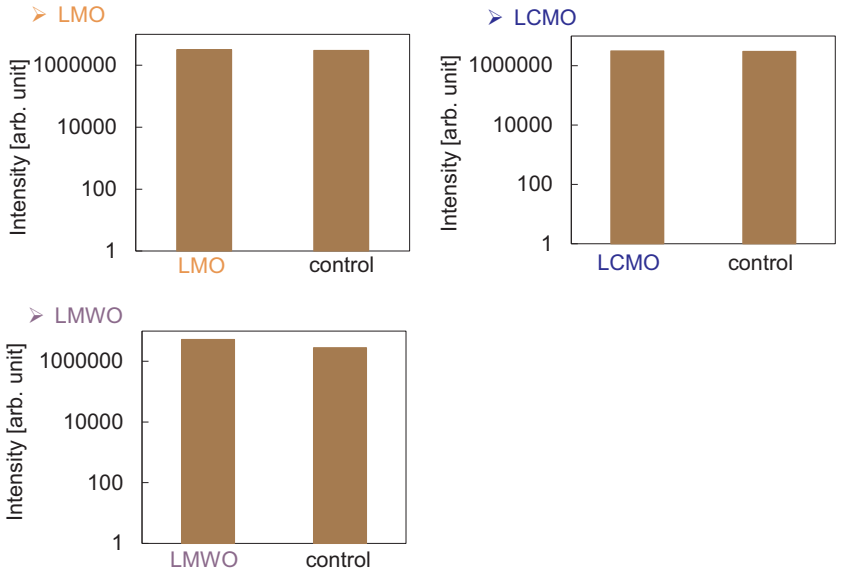

Fig. 8. Results of cytotoxicity tests for LMO, LCMO, and LMWO.

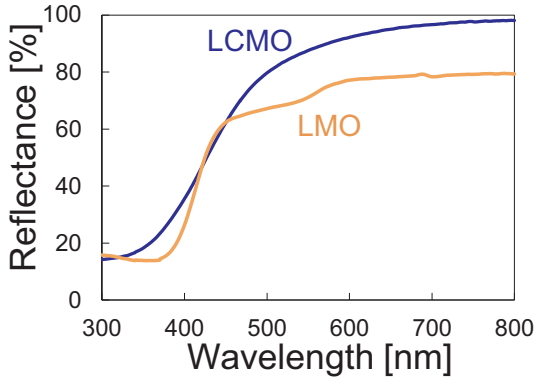

Fig. 9. UV–Vis spectra of LMO and LCMO.

Appendix A. Supplementary data

Supplementary data to this article can be found online at https://doi.org/10.1016/j.msec.2020.111323.

References

[1] S. Galdiero, A. Falanga, M. Vitiello, M. Cantisani, V. Marra, M. Galdiero, Silver nanoparticles as potential antiviral agents, Molecules 16 (2011) 8894–8918.
[2] K. Zodrow, L. Brunet, S. Mahendra, D. Li, A. Zhang, Q. Li, P.J.J. Alvarez, Polysulfone ultrafiltration membranes impregnated with silver nanoparticles show improved biofouling resistance and virus removal, Water Res. 43 (2009) 715–723.
[3] S. Gaikwad, A. Ingle, A. Gade, M. Rai, A. Falanga, N. Incoronato, L. Russo, S. Galdiero, M. Galdiero, Antiviral activity of mycosynthesized silver nanoparticles against herpes simplex virus and human parainfluenza virus type 3, Int. J. Nanomedicine 8 (2013) 4303–4314.
[4] R. Nakano, H. Ishiguro, Y. Yao, J. Kajioka, A. Fujishima, K. Sunada, M. Minoshima, K. Hashimoto, Y. Kubota, Photocatalytic inactivation of influenza virus by titanium dioxide thin film, Photochem. Photobiol. Sci. 11 (2012) 1293–1298.
[5] C. Zhanga, Y. Li, D. Shuai, Y. Shen, D. Wang, Progress and challenges in photocatalytic disinfection of waterborne viruses: a review to fill current knowledge gaps, Chem. Eng. J. 355 (2019) 399–415.
[6] H. Ghaffari, A. Tavakoli, A. Moradi, A. Tabarraei, F. Bokharaei-Salim, M. Zahmatkeshan, M. Farahmand, D. Javanmard, S.J. Kiani, M. Esghaei, V. Pirhajati-Mahabadi, A. Ataei-Pirkooh, S.H. Monavari, Inhibition of H1N1 influenza virus infection by zinc oxide nanoparticles: another emerging application of nanomedicine, J. Biomedical Sci. 26 (70) (2019) 1–10.
[7] K. Motoike, S. Hirano, H. Yamana, T. Onda, T. Maeda, T. Ito, M. Hayakawa, Antiviral activities of heated dolomite powder, Biocontrol Sci. 13 (2008) 131–138.
[8] G. Azimi, R. Dhiman, H.M. Kwon, A.T. Paxson, K.K. Varanasi, Hydrophobicity of rare-earth oxide ceramics, Nat. Mater. 12 (4) (2013) 315–320.
[9] D.J. Preston, N. Miljkovic, J. Sack, R. Enright, J. Queeney, E.N. Wang, Effect of hydrocarbon adsorption on the wettability of rare earth oxide ceramics, Appl. Phys. Lett. 105 (1) (2014) 11601.
[10] S. Sankar, B.N. Nair, T. Suzuki, G.M. Anilkumar, M. Padmanabhan, U.N.S. Hareesh, K.G. Warrier, Hydrophobic and metallophobic surfaces: highly stable non-wetting inorganic surfaces based on lanthanum phosphate nanorods, Sci. Rep. 6 (1) (2016) 22732.
[11] G. Carchini, M.G. Melchor, Z. Łodziana, N. López, Understanding and tuning the intrinsic hydrophobicity of rare-earth oxides: a DFT + U study, ACS Appl. Mater. Interfaces 8 (1) (2016) 152–160.
[12] K.K. Oh, L. Kangsik, K. Zonghoon, Y.L. Kyung, W.L. Chang, J.M. Su, M.L.M. Jae, N. Clement, D. Wontae, K. Christian, L. Hyungjun, B.R. Han, Hydrophobicity of rare earth oxides grown by atomic layer deposition, Chem. Mater. 27 (1) (2015) 148–156.
[13] N. Desai, S. Mali, V. Kondalkar, R. Mane, C. Hong, P. Bhosale, Chemically grown MoO_3 nanorods for antibacterial activity study, J. Nanomed. Nanotechnol. 6 (6) (2015) 1000338.
[14] C. Zollfrank, K. Gutbrod, P. Wechsler, J.P. Guggenbichler, Antimicrobial activity of transition metal acid MoO_3 prevents microbial growth on material surfaces, Mater. Sci. Eng. C 32 (1) (2012) 47–54.
[15] K. Krishnamoorthy, M. Premanathan, M. Veerapandian, S.J. Kim, Nanostructured molybdenum oxide-based antibacterial paint: effective growth inhibition of various pathogenic bacteria, Nanotechnology 25 315101 (2014) 1–10.
[16] C.C. Mardare, A.W. Hassel, Investigations on bactericidal properties of molybdenum–tungsten oxides combinatorial thin film material libraries, ACS Comb. Sci. 16 (11) (2014) 631–639.
[17] R.A. Rocha, E.N.S. Muccillo, Synthesis and thermal decomposition of a polymeric precursor of the $La_2Mo_2O_9$ compound, Chem. Mater. 15 (22) (2003) 4268–4272.
[18] T. Matsumoto, K. Sunada, T. Nagai, T. Isobe, S. Matsushita, H. Ishiguro, A. Nakajima, Preparation of hydrophobic $La_2Mo_2O_9$ ceramics with antibacterial and antiviral properties, J. Hazard. Mater. 378 (2019) 120610.
[19] A. Arumugama, C. Karthikeyan, A.S.H. Hameed, K. Gopinath, S. Gowri, V. Karthika, Synthesis of cerium oxide nanoparticles using *Gloriosa superba* L. leaf extract and their structural, optical and antibacterial properties, Mater. Sci. Eng. C 49 (2015) 408–415.
[20] A. Gupta, S. Das, C.J. Neala, S. Seal, Controlling the surface chemistry of cerium oxide nanoparticles for biological applications, J. Mater. Chem. B 4 (2016) 3195–3202.
[21] Y.-F. Goh, A.Z. Alshemary, M. Akram, M.R.A. Kadir, R. Hussain, In-vitro characterization of antibacterial bioactive glass containing ceria, Ceram. Int. 40 (2014) 729–737.
[22] P. Bellio, C. Luzi, A. Mancini, S. Cracchiolo, M. Passacantando, L.D. Pietro, M. Perilli, G. Amicosante, S. Santucci, G. Celenza, Cerium oxide nanoparticles as potential antibiotic adjuvant. Effects of CeO_2 nanoparticles on bacterial outer membrane permeability, BBA – Biomembranes 1860 (2018) 2428–2435.
[23] M. Mizutani, T. Isobe, S. Matsushita, A. Nakajima, Preparation of visible light photocatalyst by interface reaction between tungsten–molybdenum oxide and copper clusters, Mater. Lett. 186 (2017) 135–137.
[24] A. Arzola-Rubio, J. Camarillo–Cisneros, L. Fuentes–Cobas, V. Collins-Martinez, L. De la Torre-Saenz, F. Paraguay-Delgado, Enhanced optical properties of $W_{1-x}Mo_xO_3{\cdot}0.33H_2O$ solid solutions with tunable band gaps, Superlattice. Microst. 81 (2015) 175–184.
[25] A.B. Yousaf, M. Imran, M. Farooq, P. Kasak, Interfacial phenomenon and nanostructual enhancements in palladium loaded lanthanum hydroxide nanorods for heterogeneous catalytic applications, Sci. Rep. 8 (2018) 4354.

[26] Y.V. Plyuto, I.V. Nabich, I.V. Plyuto, A.D. Langeveld, J.A. Moulijn, XPS studies of MoO_3/Al_2O_3 and MoO_3/SiO_2 systems, Appl. Surf. Sci. 119 (1997) 11–18.

[27] Y. Baek, K. Yong, Controlled growth and characterization of tungsten oxide nanowires using thermal evaporation of WO_3 powder, J. Phys. Chem. C 111 (2007) 1213–1218.

[28] E. Paparazzo, Use and mis-use of X-rayphotoemission Ce3d spectra of Ce_2O_3 and CeO_2, J. Phys. Condens. Matter 30 (2018) 343003.

[29] F. Larachi, J. Pierre, A. Adnot, A. Bernis, Ce 3d XPS study of composite $Ce_xMn_{1-x}O_{2-y}$ wet oxidation catalysts, Appl. Surf. Sci. 195 (2002) 236–250.

[30] Y. Inaba, K. Ishikawa, K. Tatenuma, E. Ishitsuka, Development of ^{99}Mo production technique by solution irradiation method characterization of aqueous mlybdate slutions, At. Energy Soc. Jpn. 8 (2) (2009) 142–153 (in Japanese).

[31] M. Takaya, Y. Shinohara, F. Serita, M. Ono-Ogasawara, N. Otaki, T. Toya, A. Takata, K. Yoshida, N. Kohyama, Dissolution of fnctional mterials and rare earth oxides into pseudo-alveolar fluid, Ind. Health 44 (4) (2006) 639–644.

[32] J.A. Dean (Ed.), Lange's Handbook of Chemistry, 12th edition, McGraw-Hill Book Company, New York, 1978pp 4-38 and 4-125.

[33] S.G. Sarafianos, U. Kortz, M.T. Pope, M.J. Modak, Mechanism of polyoxometalate-mediated inactivation of DNA polymerases: an analysis with HIV-1 reverse transcriptase indicates specificity for the DNA-binding cleft, Biochem. J. 319 (2) (1996) 619–626.

[34] Y. Inouye, Y. Tokutake, T. Yoshida, Y. Seto, H. Hujita, K. Dan, A. Yamamoto, S. Nishiya, T. Yamase, S. Nakamura, In vitro antiviral activity of polyoxomolybdates. Mechanism of inhibitory effect of PM-104 $(NH_4)_{12}H_2(Eu_4(MoO_4(H_2O)_{16}(Mo_7O_{24})_4)\cdot 13H_2O$ on human immunodeficiency virus type 1, Antiviral Res. 20 (4) (1993) 317–331.

[35] M.S. Weeks, C.L. Hill, R.F. Schinazi, Synthesis, characterization, and anti-human immunodeficiency virus activity of water-soluble salts of polyoxotungstate anions with covalently attached organic groups, J. Med. Chem. 3 (35) (1992) 1216–1221.

[36] K. Dan, K. Miyashita, Y. Seto, H. Fujita, T. Yamase, The memory effect of heteropolyoxotungstate (PM-19) pretreatment on infection by herpes simplex virus at the penetration stage, Pharmacol. Res. 46 (4) (2002) 357–362.

[37] D.A. Judd, J.H. Nettles, N. Nevins, J.P. Snyder, D.C. Liotta, J. Tang, J. Ermolieff, R.F. Schinazi, C.L. Hill, Polyoxometalate HIV-1 protease inhibitors. A new mode of protease inhibition, J. Am. Chem. Soc. 123 (5) (2001) 886–897.

[38] H. Goto, A novel function of plasminogen-binding activity of the NA determines the pathogenicity of influenza A virus, Virus 54 (4) (2004) 83–91 (in Japanese).

[39] G. Sutton, J.M. Grimes, D.I. Stuart, P. Roy, Bluetongue virus VP4 is an RNA-capping assembly line, Nat. Struct. Mol. Biol. 14 (5) (2007) 449–451.

[40] R. Golmohammadi, K. Fridborg, M. Bundule, K. Valegård, L. Liljas, The crystal structure of bacteriophage Qβ at 3.5 Å resolution, Structure 4 (1996) 543–554.

[41] Takahiko Makino, Ph.D. thesis, Tungsten Recycling From Cemented Carbide Scraps by Metal - Biotechnology, Hiroshima Univ. Japan, 2018.

[42] A. Yamamoto, K. Adachi, Label-free colorimetric sensing of α-amino acids based on surface-enhanced photochromic phenomena of molybdenum (VI) oxide nanoparticles, Bunseki Kagaku 66 (9) (2017) 639–646.

[43] T. Ogi, T. Makino, S. Nagai, W.J. Stark, F. Iskandar, K. Okuyama, Facile and efficient removal of tungsten anions using lysine-promoted precipitation for recycling high-purity tungsten, ACS Sustain. Chem. Eng. 5 (4) (2017) 3141–3147.

[44] J.F. Pérez, M.-C. Ruiz, M.E. Chemello, F. Michelageli, Characterization of a membrane calcium pathway induced by rotavirus infection in cultured cells, J. Virology 73 (1999) 2481–2490.

[45] G. Wengler, G. Wengler, A. Koschinski, A short treatment of cells with the lanthanide ions La^{3+}, Ce^{3+}, Pr^{3+} or Nd^{3+} changes the cellular chemistry into a state in which RNA replication of flaviviruses is specifically blocked without interference with host-cell multiplication, J. General Virology 88 (2007) 3018–3026.

[46] Y.-N. Liu, S. Shi, W.-J. Mei, C.-P. Tan, L.-M. Chen, J. Liu, W.-J. Zheng, L.-N. Ji, In vitro and in vivo investigations of the antiviral activity of a series of mixed-valence rare earth borotungstate heteropoly blues, Eur. J. Med. Chem. 43 (2008) 1963–1970.

[47] J. Liu, W.-J. Mei, A.-W. Xu, C.-P. Tan, S. Shi, L.-N. Ji, Synthesis, characterization and antiviral activity against influenza virus of a series of novel manganese-substituted rare earth borotungstates heteropolyoxometalates, Antivir. Res. 62 (2004) 65–71.

[48] D.L. Barnarda, C.L. Hill, T. Gage, J.E. Matheson, J.H. Huffman, R.W. Sidwell, M.I. Otto, R.F. Schinazi, Potent inhibition of respiratory syncytial virus by polyoxometalates of several structural classes, Antivir. Res. 34 (1997) 27–37.

[49] M. Lykaki, E. Pachatouridou, S.A.C. Carabineiro, E. Iliopoulou, C. Andriopoulou, N. Kallithrakas-Kontose, S. Boghosian, M. Konsolakisa, Ceria nanoparticles shape effects on the structural defects and surface chemistry: implications in CO oxidation by Cu/CeO_2 catalysts, Appl. Catal. B Environ. 230 (2018) 18–28.

[50] S. Scirè, S. Minicò, C. Crisafulli, C. Satriano, A. Pistone, Catalytic combustion of volatile organic compounds on gold/cerium oxide catalysts, Appl. Catal. B Environ. 40 (2003) 43–49.

[51] M. Shiohara, T. Isobe, S. Matsushita, A. Nakajima, Decomposition of 2-naphthol in water by TiO2 modified with MnOx and CeOy, Mater. Chem. Phys. 183 (2016) 37–43.

[52] C. Kato, M. Shiohara, K. Sunada, T. Isobe, A. Yamaguchi, S. Matsushita, H. Ishiguro, M. Miyauchi, A. Nakajima, Decomposition of 2-naphthol in water and antibacterial property by NiO and CeO_x modified TiO_2 in the dark or under visible light, J. Ceram. Soc. Jpn. 127 (2019) 688–695.

[53] F.J. Jing, N. Huang, Y.W. Liu, W. Zhang, X.B. Zhao, R.K.Y. Fu, J.B. Wang, Z.Y. Shao, J.Y. Chen, Y.X. Leng, X.Y. Liu, P.K. Chu, Hemocompatibility and antibacterial properties of lanthanum oxide films synthesized by dual plasma deposition, J. Biomed. Mater. Res. Part A 87A (2008) 1027–1033.

[54] J. He, W. Wang, W. Shi, F. Cui, La_2O_3 nanoparticle/polyacrylonitrile nanofibers for bacterial inactivation based on phosphate control, RSC Adv. 6 (2016) 99353–99360.

[55] J. Liu, G. Wang, L. Lu, Y. Guo, L. Yang, Facile shape-controlled synthesis of lanthanum oxide with different hierarchical micro/nanostructures for antibacterial activity based on phosphate removal, RSC Adv. 7 (2017) 40965–40972.

[56] B. Alberts, D. Bray, K. Hopkin, Essential Cell Biology, fourth edition, (2016) translated by K. Nakamura and K. Matsubara, Nankodo, Japan, Chapter 4.

[57] K. Sunada, M. Minoshima, K. Hashimoto, Highly efficient antiviral and antibacterial activities of solid-state cuprous compounds, J. Hazard. Mater. 235–236 (2012) 265–270.

[58] M. Minoshima, Y. Lu, T. Kimura, R. Nakano, H. Ishiguro, Y. Kubota, K. Hashimoto, K. Sunada, Comparison of the antiviral effect of solid-state copper and silver compounds, J. Hazard. Mater. 312 (2016) 1–7.

[59] J.A. Dean (Ed.), Lange's Handbook of Chemistry, 12th edition, McGraw-Hill Book Company, New York, 1978, pp. 4–107.

[60] H.S. Yogananda, H. Nagabhushana, G.P. Darshan, R.B. Basavaraj, B. Daruka Prasad, M.K. Sateesh, G.K. Raghu, MoO_3 nanostructures from EGCG assisted sonochemical route: evaluation of its application towards forensic and photocatalysis, J. Alloys Compound. 745 (15) (2018) 874–891.

[61] X. Zhang, L. Wang, E. Levänen, Superhydrophobic surfaces for the reduction of bacterial adhesion, RSC Adv. 3 (30) (2013) 12003–12020.

[62] I. Mannelli, R. Reigada, I. Suárez, D. Janner, A. Carrilero, P. Mazumder, F. Sagués, V. Pruneri, M. Lakadamyali, Functionalized surfaces with tailored wettability determine influenza A infectivity, ACS Appl. Mater. Interfaces 8 (2016) 15058–15066.

[63] H. Badani, R.F.G. William, C. Wimley, Peptide entry inhibitors of enveloped viruses: the importance of interfacial hydrophobicity, Biochim. Biophys. Acta 1838 (2014) 2180–2197.

[64] R. Li, S. Yabe, M. Yamashita, S. Momose, S. Yoshida, S. Yin, T. Sato, Synthesis and UV-shielding properties of ZnO- and CaO-doped CeO_2 via soft solution chemical process, Solid State Ionics 151 (2002) 235–241.

[65] F. Caputo, M. De Nicola, A. Sienkiewicz, A. Giovanetti, I. Bejarano, S. Licoccia, E. Traversa, L. Ghibelli, Cerium oxide nanoparticles, combining antioxidant and UV shielding properties, prevent UV-induced cell damage and mutagenesis, Nanoscale 7 (2015) 15643–15656.

[66] M. Aguirre, M. Paulis, J.R. Leiza, UV screening clear coats based on encapsulated CeO_2 hybrid latexes, J. Mater. Chem. A 1 (2013) 3155–3162.